Simulations of shear in gouge zones

Einat Aharonov[(1)], David W. Sparks[(2)]

(1) Weizmann Institute of Science, Department of Environmental Sciences, Rehovot 76100(e-mail: einata@wicc.weizmann.ac.il phone: 972-8-9344228; fax: 972-9-9344124). (2) Dept of Geology and Geophysics, Texas A&M University, College Station, TX, USA. (e-mail:sparks@seaver.tamu.edu, phone:979-458-1051)

Abstract

We present results from two-dimensional computer simulations of shearing granular materials, using a molecular dynamics model. We find that there are two distinct modes of deformation of granular materials under shear - "solid-like" characterized by diffuse shear and/or internal shear bands, and "fluidized", characterized by persistent boundary layer shear. Deformation mode is controlled by normal confining stress, system size and velocity, and possibly by other factors like grain shape etc. The velocity profile is predicted theoretically. The two modes of deformation are characterized by different micromechanical measures, but do not differ in macroscopic measures. The behavior of the weak contacts, and not the stress chains, determine the overall behavior of the system. This has strong implications to stick and slip in granular materials as explained in Sparks and Aharonov, this issue.

Introduction

In recent years there has been much work on granular dynamics, with emphasis on the resemblance of grain aggregates to solids or fluids, depending on the conditions of the deformation. In relation to Earthquakes, gouge zones are sometimes thought to be "fluidized" during rupture and theorized to have in this state high porosity, and a low apparent friction. Little is actually known about this type of behavior since most geophysics experiments result in "solid-like" deformation, e.g. [1, 2], seen under slow shear and high normal stress. This second type of behavior results in either diffuse deformation or formation of internal shear bands. Understanding the response of the micro and macromechanics to different boundary conditions will help understand the dynamics of granular materials in general, and gouge zones in particular. Since computer models allow easy excess to a large range of normal stresses and system sizes, modeling these systems enables investigation of the phase space and understanding of the global behavior.

We numerically model grain aggregates using a version of the 'discrete element method' [4, 5] which treats grains as inelastic disks with rotational and translational degrees of freedom. The numerical model and conditions we use are similar to our previous work [3]. When the distance between the centers of any two grains is less than the sum of their radii, the grains undergo an inelastic interaction. During the interaction the grains experience a contact force that has both shear and normal components. The normal component consists of a linear elastic repulsive force and a damping force dependent on the relative grain velocities. Shear forces on contacts are determined using an elastic/friction law [4]. Time is measured in units of undissipated elastic wave travel time, and distance in units of average disk diameter. We use non-dimensional units from here on. Simulations are performed on rectangular systems with $nt = nx \times ny$ disks. The top and bottom edges of the box are composed of grains

glued together to form rigid rough walls of length nx (Figure 1). The box is periodic in the horizontal direction. Grain radii are randomly drawn from a Gaussian distribution. The system is initiated as a tall loosely packed box, which is compacted vertically by normal stresses. After compaction and relaxation we apply a confining normal stress N to the upper and lower walls, and move the top wall in the x direction by applying a constant velocity V_0. The system then evolves spontaneously to have a more or less constant porosity.

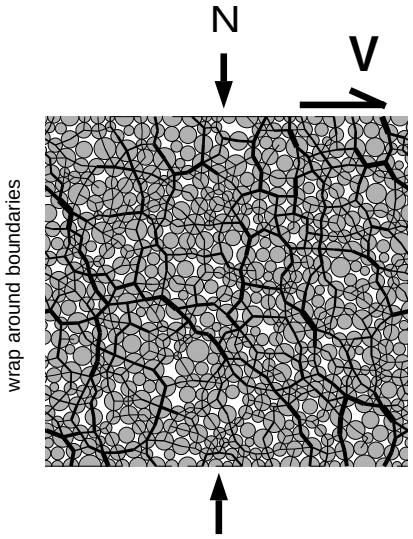

Figure 1: A representative numerical simulation of a granular aggregate. This system contains approximately 24 x 24 grains, shown as circles. The direction and magnitude of contact forces between grains is shown by black lines.

Simulation results

shear profiles

Applying different normal stresses results in different shear profiles, and different overall behavior. The low end of the normal stress regime ($N = 1e-6$ in non-dimensional units which is equivalent to $N = 60kPa$ for glass beads of size 1mm) corresponds to the regime in which some laboratory experiments [6] are performed: grains suffer little deformation, and indeed stresses are low enough to generally not result in grain breakage under experimental conditions. The highest normal stress we used ($N = 1e-3$, equivalent to $N = 60MPa$) is appropriate for geophysical simulations, corresponding to a burial depth of 2 km. Under the highest normal stresses, some of our numerical grains suffer a small "elastic deformation" approaching 0.5% of a grain diameter. In experiments of shear in rocks or glass beads grain breakage often occurs at these stresses [7].

Under low load all deformation is localized near the moving boundary, (in agreement with experiments [6]) and it remains there for the duration of the run. In contrast, under high normal stresses deformation is either diffuse with nearly evenly distributed shear, or localized in shear bands which can appear at any depth. The shear bands have a characteristic width of 10-20 grains. Under high normal load the system spends about half the time in localized motion and the other half in distributed shear. The location of an individual shear band may persist for times ranging between 250-25000 time-steps, which is equivalent to motion of the

upper wall over a distance of 0.2-20 grain diameters. Once a shear band dies a new one may appear at any subsequent time and at any depth. The distribution, duration and location of localization events is not trivial and merits future studies.

We use the terms "fluidized" or "solid-like" to distinguish simulations in which shear rate decreases consistently with distance from the moving boundary, from those in which internal shear bands or diffuse shear appear. We look at long time averages (over $2 * 10^6$

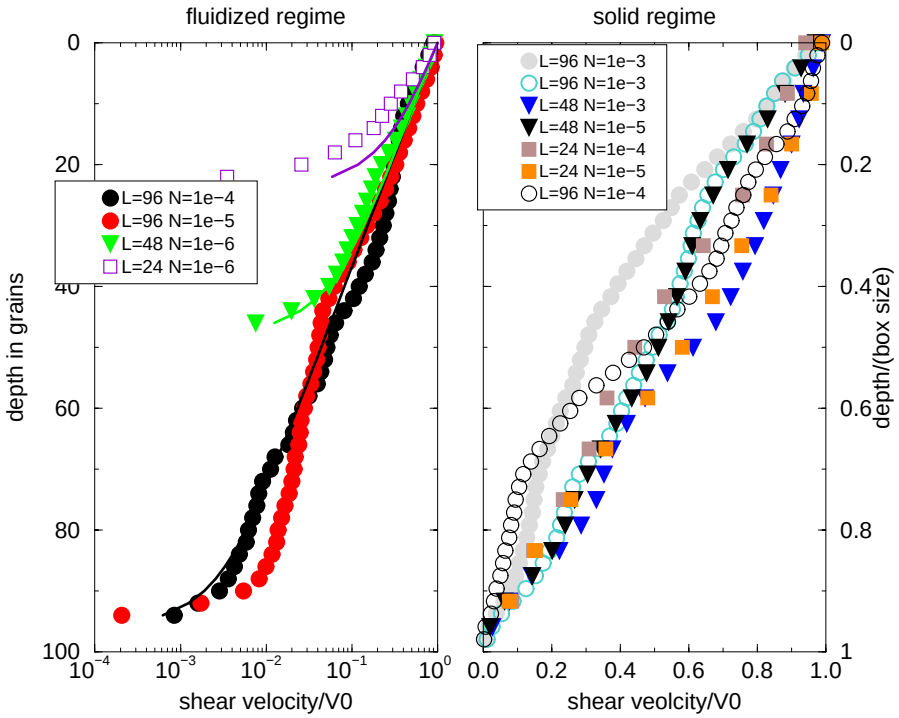

Figure 2: Long-time averages of boundary parallel (horizontal) grain velocities as function of depth. Open symbols are from runs with $v_0 = 10^{-4}$ and closed from runs with $v_0 = 10^{-3}$. Note that velocity axis is logarithmic for the fluidized runs and linear for the solid-like runs. Three different box heights, $ny = L = 24, 48, 96$, were used, as well as confining loads ranging between $N = 10^{-6} - 10^{-3}$.

time steps, or an upper wall displacement of about 100 grains) of the horizontal component of grain velocities, plotted as function of distance from the shearing wall (Figure 2). In solid-like simulations (Figure 2 right panel) long time averaging of grain velocities shows completely distributed shear. Mean horizontal grain velocities decay nearly linearly away from the moving boundary, demonstrating that transient shear bands in the system truly occur at random depths, which over time average out to a uniform shear. Note that in natural systems breaking may lock the shear bands in one position. In fluidized simulations (Figure 2 left panel) velocity decays roughly exponentially away from the moving boundary.

We fit the fluidized velocity profiles in the left panel using a theoretical prediction which assumes that grain fluctuations (granular temperature) result from shear created by the moving boundary. This "heat" diffuses away from the energy source and into the layer. Details of the calculation are given in [8], and are shown there to also agree with experiments performed under low confining load. The basics of this theory is applicable also to the solid regime, but fitting of theory to simulation profiles is complicated by the transient internal shear.

phase diagram

The box height (layer thickness in units of average grain diameter) is important in determining where the transition between the solid-like and fluid-like behaviors occurs- the taller the box the easier it is to fluidize (figure 2). Figure 3 schematically shows the phase diagram in box

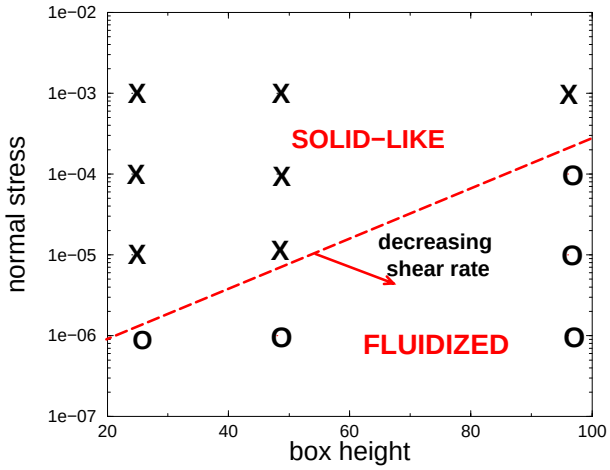

Figure 3: Schematic phase space for the two different behaviors of the system: fluidized(O) or solid-like (X). As the box gets bigger it is easier to liquefy the aggregate even under higher normal stresses. Wall velocity also effects the phase boundary.

size versus confining normal stress. In all the runs, boundary velocity, V_0, was set to 10^{-3}. We see an indication that increasing shear velocity will cause the phase boundary to migrate to the left.

It is curious that there is not much difference between macroscopic measures obtained from systems with the boundary shears and systems with internal shears. For example, the variation of time-averaged porosity among all the simulations is less than one percent, and the variation is not systematic. Porosity in low normal stress runs may be either higher or lower than porosity in high normal stress runs, depending on the individual runs.

Micromechanics

It is now recognized that force and velocity heterogeneities exist on all scales in granular systems [9, 10]. The largest contact forces between two grains is typically several times the mean force in the system. The contact forces have an exponential probability distribution, with the rarer highly-stressed contacts grouped in a network of intersecting lines of particles termed force chains [11]. We show that micromechanical measures, obtained from measurements on individual contacts, are good predictors for the emerging rheologies. In this section we present results from two test runs using a box of $96 * 48$. A solid-like case with confining stress of $N = 10^{-3}$ and a liquid-like case with $N = 10^{-5}$. We look at a subset of contacts between grains carrying a normalized force (normalized by the mean contact force in the system) smaller than a cutoff value ($f < \xi$), and call this subset the "ξ network". For example forces belonging to the network of $\xi = 1$ are forces smaller than the mean force. We follow closely the method suggested by [10].

The contact network that forms is characterized by the probability density function $E(\theta, \xi)$ of finding contact with direction θ in the ξ network. The contact angle θ is measured from the horizontal axis. $E(\theta)$ may be represented by a Fourier series containing even components

and can be written as [10] $E(\theta, \xi) = 0.5(1 + A_c(\xi)\cos(\theta - \theta_c(\xi)))$. The coefficient A_c is the amplitude of anisotropy, while θ_c is the principal direction of the contacts in the ξ network. In both solid and fluidized cases the direction of anisotropy of the entire set of contacts (i.e.

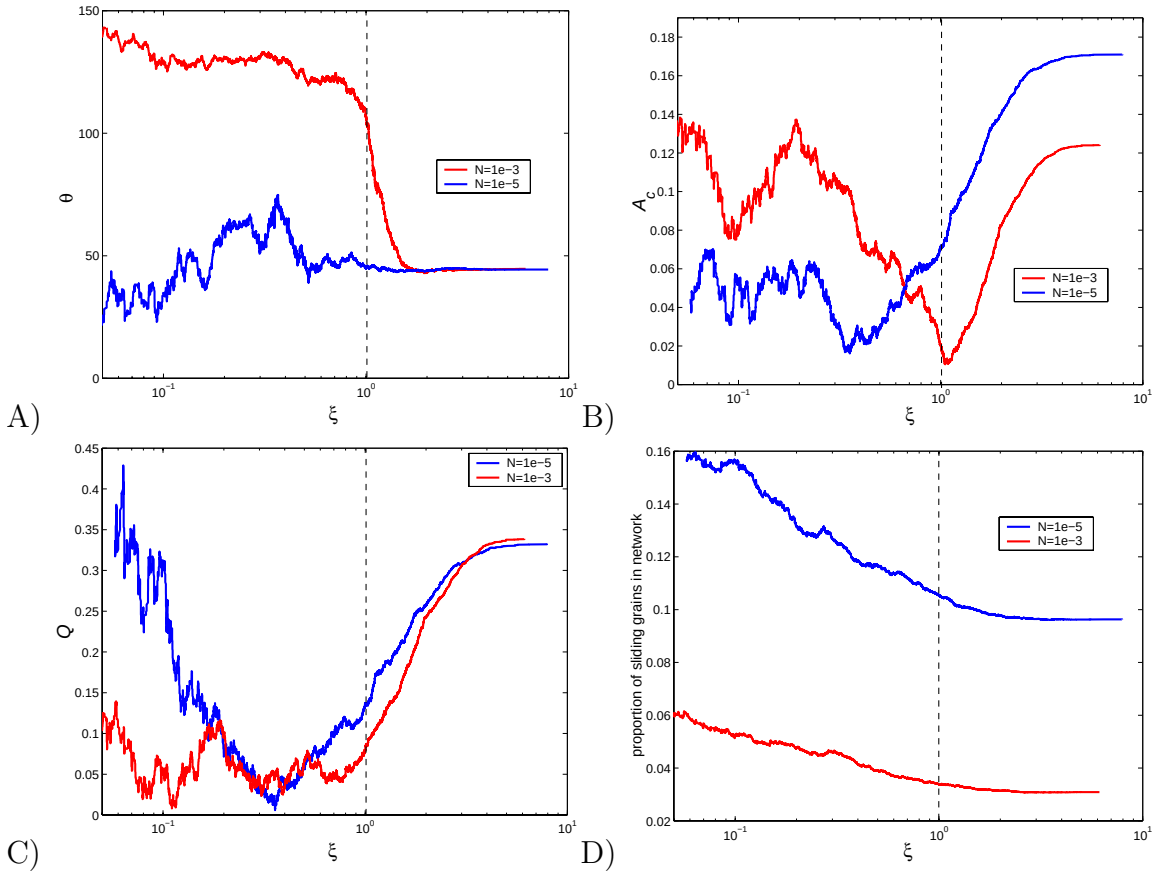

Figure 4: a) Principal contact directions θ_c b) Amplitude of anisotropy A_c, c) The deviatoric stress Q, d) Proportion of sliding contacts in the ξ network for the liquid case, blue, $N = 10^{-5}$, and solid case, red, $N = 10^{-3}$

at $\xi \to \infty$) is about 45 degrees from horizontal (Figure 4 A), in the expected direction of maximum compression. This direction is due to orientation of the "strong" contacts, those in force chains. Surprisingly, the difference between the solid and fluidized cases is in the weak contacts $\xi < 1$. In the solid case there exists a bimodal distribution of contact orientations: the weak forces with $\xi < 1$, have an orientation of 135 degrees, which is perpendicular to the direction of maximum compression. These are the contacts that contribute to the rigidity of the system and prevent buckling of the chains. In the fluidized system, the weak contacts do not provide the rigidity required for the system, since they are not oriented at the normal direction to the strong contacts and therefor there is no "mesh" which can be a rigid structure, but just a collection of rods, which can freely rotate. In viewing the direction of contacts the degree of anisotropy A_c must also be considered (Figure 4 B). $A_c = 0$ means randomly distributed contacts and any value of θ_c in cases of a small A_c is not meaningful. In the solid case the degree of anisotropy is large for the weak contacts and for the entire contact network. For the fluidized system, the anisotropy is less pronounced for all of the $\xi < 1$ networks, i.e. the weak contacts are more randomly arranged.

The deviatoric load, $Q = (\sigma_1 - \sigma_2)/(\sigma_1 + \sigma_2)$, carried by the ξ network also is different between solid and liquid cases. Figure 4 C shows that although the total deviatoric load the system carries (i.e. $\xi \to \infty$) in the fluid-like and solid-like systems are the same, the solid

system has a bimodal distribution of contacts, with strong contacts $\xi > 1$ carrying the load, while the weak phase behaves as an interstitial fluid which supports only the pressure. In the system under the lower confining load the deviatoric load is carried also by the weakest contacts, and there is no bi-modal distribution.

When investigating the proportion of sliding contacts, Figure 4D, in both systems a larger proportion of the weak contacts slip than the strong contacts. It is not surprising, since they will be closer to the Coulomb sliding condition at any given shear stress value, since the normal force on them is smaller. This is in agreement with simple shear [10] simulations. However what is surprising is that frictional slip is prevalent much more in the liquid system than the solid system. It is common to refer the more gas like systems as collision-controlled and the more solid like systems as frictional controlled. It is interesting that this approach is intuitive but erroneous- in the liquid systems much more friction dissipation is going on than in the solid systems, where perhaps rolling is a prevalent mode of deformation. This is also consistent with the fact that the solid-like simulations have a slightly lower apparent friction than the fluid-like simulations (again, somewhat contrary to prevalent ideas).

References

[1] C. Marone and B. E. Hobbs and A. Ord, 1992, *Contrasts in frictional behavior for distributed and localized shear,* Pure Appl. Geophys.**139**, 195-214.

[2] N. Beeler and T. Tullis, 1997, *The roles of time and displacement in velocity dependent volumetric strain of fault,* J. Geophys. Res.**102**, 22,595-22,610.

[3] E. Aharonov and D. Sparks, 1999, *Rigidity phase transition in granular packings,* Phys. Rev. E **60**, 6890-6896.

[4] P. A. Cundall and O. D. Strack, 1979, *A discrete numerical model for granular assemblies,* Geotechnique, **29**, 47-65

[5] F. Donze and P. Mora and S. A. Magnier, 1994, *Numerical simulation of faults and shear zones,* Geophys. J. Int, **116**, 46-52

[6] S. Nasuno and A. Kudrolli and J. Gollub, 1997, *Friction in granular layers: hysteresis and precursors,* Phys. Rev. Lett., **79**, 4780-4784

[7] S. B. Savage and M. Sayed, 1984, *Stresses developed by dry cohesionless granular sheared in an annular shear cell,* J. fluid Mech., **142**, 391-430

[8] W. Losert and L. Bocquet and T.C. Lubensky and J.P. Gollub, 2000, *Particle dynamics in sheared granular material*, Phys. Rev. Lett., **85**, 1428-1431

[9] B. Miller and C. O'Hern and R.P. Behringer, 1996, *Stress flactutations for continuously sheared granular materials*, Phys. Rev. Lett., **77**, 3110-3113

[10] F. Radjai and D. E. Wolf and M. Jean and J. J. Moreau, 1998, *Bimodal character of stress transmission in granular packings*, Phys. Rev. Lett., **80**, 61-64

[11] S. J. Steacy and C. G. Sammis, 1994, *The micromechanics of friction in a granular layer*, Pure Appl. Geophys, **142**, 777-794